Clays and Clay Minerals, Vol. 58, No. 2, 174–187, 2010.

DENSITY FUNCTIONAL THEORY (DFT) STUDY OF THE HYDRATION STEPS OF $Na^{+}/Mg^{2+}/Ca^{2+}/Sr^{2+}/Ba^{2+}$-EXCHANGED MONTMORILLONITES

Abid Berghout[1], Daniel Tunega[2,3], and Ali Zaoui[1,*]

[1] Laboratoire de Génie Civil et géo-Environment (EA 4515) Lille Nord de France, Ecole Polytechnique de Lille, Université des Sciences et Technologie de Lille, Cité Scientifique, Avenue Paul Langevin, 59655 Villeneuve d'Ascq Cedex, France
[2] Institute for Theoretical Chemistry, University of Vienna, Währinger Straße 17, A-1090 Vienna, Austria
[3] Institute of Soil Research, University of Natural Resources and Applied Life Sciences Vienna, Peter-Jordan-Straße 82, A-1190 Vienna, Austria

Abstract—Theoretical models of the mechanical properties of hydrated smectites, saturated with a variety of cations, are of much value in determining the potential for their use in various applications, including clay-polymer nanocomposites, but the development of such models is still in its infancy. The purpose of this study was to calculate the effects of divalent cations on the structural and mechanical elasticity of montmorillonite under different degrees of hydration. A theoretical study of the swelling and hydration behavior of montmorillonite was, therefore, undertaken using density functional theory (DFT) to investigate the basal spacing behavior of the homoionic montmorillonite with varying amounts of water in the interlayer space. The effect of the degree of the hydration of divalent interlayer cations ($Mg^{2+}/Ca^{2+}/Sr^{2+}/Ba^{2+}$) on the structure expansion of the interlayer space was analyzed. In addition, the results obtained were compared to calculations performed on the montmorillonite model with a monovalent cation (Na^{+}). The basal spacing (d_{001}) is governed by the size and the degree of hydration of the countercations. The structures containing divalent cations are more compact than structures with monovalent cations. Ba-exchanged montmorillonite was found to have the largest d_{001} value for any degree of hydration ('dry,' one water layer, or two layers). The basal spacings of 'dry' montmorillonite exchanged with small cations, Mg^{2+} and Ca^{2+}, are very similar. In hydrated models, the d_{001} expansion correlates with the ionic radius of the interlayer cation. The dependence of the total electronic energy on the volume expansion was calculated. From the energetic curves, bulk modulus (B_0) was obtained by fitting in order to show how the compliance of the material depends on the type of interlayer cation and on the degree of hydration. With increasing water content in the interlayer space, the bulk modulus decreased, suggesting that the *c*-axial compression becomes easier with increasing hydration of the clay mineral. The values of the bulk modulus in hydrated systems are less sensitive to the type of the interlayer cation.

Key Words—Hydration, Density Functional Theory, Interlayer Cation, Montmorillonite.

INTRODUCTION

Clay minerals are aluminosilicates which predominate in mineral fractions of soils and sedimentary rocks (Perkins, 1998; Velde, 1995). They are also important for industrial and technological applications due to their chemical and catalytic activities, *e.g.* as sorbents, filters, or waste deposits (Giese and van Oss, 2002; Bailey, 1988). Generally, these minerals consist of one or two layers of polymerized silicon-oxygen tetrahedra and one layer of polymerized aluminum or magnesium oxygen/hydroxyl octahedra stacked on top of each other in a well defined manner (Velde, 1995). Montmorillonite belongs to the smectite family of 2:1 clay minerals; it possesses a negative layer charge, q, due to isomorphic substitutions mainly in the octahedral sheet (Mg^{2+} for Al^{3+}). Typical values of q for smectites are in the range $0.2-0.6\ |e|$. The excess negative charge is normally compensated by interlayer counterions. The cations and the charged clay mineral surface can interact strongly with polar solvents and easily undergo hydration. Smectites can exchange interlayer cations (usually in hydrated form) and also have a tendency to swell by the incorporation of large amounts of water molecules. These minerals also intercalate various organic molecules into the interlayer space.

The hydration and dehydration reactions of montmorillonite are important in many geological processes and have been linked to phenomena as diverse as sediment over pressurization and petroleum migration. Characterized by significant swelling capacities, montmorillonites are used widely for the intercalation of various species, from small molecules to polymers, into the interlayer space (Kato and Usuki, 2000). The design of new clay-polymer nanocomposites with improved mechanical (Liu *et al.*, 2003; Wan *et al.*, 2003; Zhang *et al.*, 2005), heat resistant (Qin *et al.*, 2003), or coating (Majumdar *et al.*, 2003) properties is a field of intense research. Clays are also used as molecular-sieve catalysts (Kantam *et al.*, 1998), ion exchangers, and adsorbents (Manju *et al.*, 1999).

* E-mail address of corresponding author:
azaoui@polytech-lille.fr
DOI: 10.1346/CCMN.2010.0580204

The swelling properties of clays can also be regarded as a critical drawback, *e.g.* in the field of petrologic processes. The hydration of clays may lead to borehole instabilities. In such circumstances, new additives are required to penetrate into clay materials thereby preventing them from swelling (Bains *et al.*, 2001). Numerous experimental studies on the swelling behavior of smectite minerals under different conditions can be found in the literature. An important factor which influences the swelling is the nature of the exchangeable cation in the interlayer space (Suquet *et al.*, 1975; Guindy *et al.*, 1985; Fu *et al.*, 1990; Slade *et al.*, 1991; Sato *et al.*, 1992; Bérend *et al.*, 1995; Cases *et al.*, 1997; Cuadros, 1997; Dios Cancela *et al.*, 1997; Zabat and Van Damme, 2000; Bray and Redfern, 2000; Ferrage *et al.*, 2005, 2007a, and 2007b; Abramova *et al.*, 2007). For example, experiments carried out on Ca-montmorillonite have shown that at ambient conditions of 300 K and 1 bar the d_{001} spacing of the anhydrous phase, ~9.7 Å, hydrates to an 11.2−12.4 Å one-layer hydrate, to a 15.0−15.5 Å two-layer hydrate, and to an 18.0−19.1 Å three-layer hydrate (Posner and Quirk, 1964; Keren and Shainberg, 1975; Suquet *et al.*, 1975; McEwan and Wilson, 1980; Slade *et al.*, 1991; Sato *et al.*, 1992; Cases *et al.*, 1997; Cuadros, 1997; Bray *et al.*, 1998; Bray and Redfern, 1999, 2000; Ferrage *et al.*, 2005, 2007a).

Unlike zeolites, where first-principles simulation methods have been used extensively, such studies of clays have been less common. Sainz-Díaz and co-workers studied octahedral-cation distributions in smectites and illites by means of density functional theory (DFT) methods (Sainz-Díaz *et al.*, 2002; Timon *et al.*, 2003; Botella *et al.*, 2004; Hernández-Laguna *et al.*, 2006). The relative stability of *cis*- and *trans*-vacant sites in montmorillonite models was studied by Minisini and Tsobnang (2005). Tunega *et al*. (2007) calculated the relative stabilities of different structural arrangements in dioctahedral phyllosilicates. Only a few *ab initio* studies have been devoted to hydrated phases of smectites. The effect of exchangeable cations on the swelling properties of 2:1 dioctahedral clays was investigated by means of a periodic, first-principles study, where a series of mono- and divalent cations was used (Chatterjee *et al.*, 2004; Chatterjee, 2005). *Ab initio* molecular dynamics (AIMD) was used in the study of the hydration of a Na-smectite (Boek and Sprik, 2003). Constrained AIMD has also been used in the study of the adsorption of a Na^+ ion on a smectite clay (Suter *et al.*, 2008).

The swelling and hydration of smectite minerals has been studied extensively by means of empirical force-field methods. The Monte Carlo (MC) simulation method has been used to study water confined between the layers of 2:1 clay minerals (Skipper *et al.*, 1991) and an interlayer structure in swelling clay minerals containing hydrated homoionic cations (Skipper *et al.*, 1995a, 1995b; Chang *et al.*, 1995; Boek *et al.*, 1995; Park and Sposito, 2000; Skipper *et al.*, 2006). The MC method has also been used to predict the interlayer basal separations of Na- and Ca-saturated Wyoming clays at a constant stress set of conditions and at constant chemical potential (Chávez-Páez *et al.*, 2001a, 2001b). Swelling of Na- and Cs-montmorillonites has been studied by means of MC and molecular dynamics (MD) simulations (Marry *et al.*, 2002). The MC simulations were applied to investigate the interlayer structure of Mg- and Ca-montmorillonite for various hydration levels (Greathouse *et al.*, 2000; Greathouse and Storm, 2002; Fang *et al.*, 2004). Molecular simulations were carried out on the grand-canonical ensemble of water and cations in Wyoming and Arizona montmorillonite clay minerals, with varying relative humidity (Tambach *et al.*, 2004). Hybrid MC and MD simulations were used in the study of Na-montmorillonite hydrates under basin conditions (Odriozola and Guevara-Rodríguez, 2004). The MC method for grand canonical and grand isoshear ensemble simulations has been used to characterize the free energy, enthalpy, and entropy in Cs-, Na-, and Sr-montmorillonite swelling (Whitley and Smith, 2004). The stability of the hydrated phases of Ca-montmorillonite was simulated using hybrid MC simulations (Odriozola and Aguilar, 2005). Series of MC simulations were performed in order to investigate the reasons for the remarkable difference in experimental swelling patterns of a natural Na-rich/Mg-poor montmorillonite and a homoionic Na-montmorillonite (Meleshyn and Bunnenberg, 2005). The state and dynamics of water and cations in pure and mixed Na-Cs-montmorillonite as a function of the interlayer water content were investigated by means of MC and classical molecular-dynamics methods (Kosakowski *et al.*, 2008).

The aim of the present work was to show by means of theoretical calculations how the type of divalent interlayer cation and the different degree of its hydration affect the structural (basal spacing, d_{001}) and mechanical-elastic (bulk modulus, B_0) properties of montmorillonite. The study of mechanical characteristics is important in terms of the preparation of new clay-polymer composites with defined properties.

STRUCTURAL AND COMPUTATIONAL METHODS

Structural models

The physical properties of smectites are closely related to details of their composition and arrangements of ions within the structures (Stucki, 1988). Complete information on the structural and compositional details of individual minerals usually cannot be obtained with standard diffraction methods because of a combination of compositional heterogeneity and the existence of different arrangements in layer stacking, although a few relatively well defined specimens have been characterized (Manceau *et al.*, 2000; Drits, 2003).

https://doi.org/10.1346/CCMN.2010.0580204 Published online by Cambridge University Press

The compositional variety and structural complexity of clay minerals usually require a certain simplification of models in molecular modeling, especially when *ab initio* methods are used. The structural models used in this work as a base for the model systems were derived from the structure of a natural smectite known as Wyoming montmorillonite (Tsipursky and Drits, 1984). This montmorillonite is a 2:1 dioctahedral smectite with the unit-cell formula $Na_{0.75}nH_2O[Si_{7.75}Al_{0.25}][Al_{3.5}Mg_{0.5}]O_{20}(OH)_4$. Initial cell parameters (a = 5.18 Å, b = 8.97 Å, c = 9.95 Å, β = 99.5º) were taken from the work by Tsipursky and Drits (1984). The present computational models use simplified composition only with Al^{3+}/Mg^{2+} substitution in the octahedral sheet and *trans*-OH coordination of the octahedral vacancy. A previous study (Tunega *et al.*, 2007) showed that the layer structure with this coordination of the vacancy was more stable than *cis*-coordination of the vacancy if only octahedral substitutions were considered. Owing to the study of divalent cations in the interlayer space, the computational cell was extended and consisted of two unit cells (extension in the *a* direction). This cell had two isomorphic Al^{3+}/Mg^{2+} substitutions and the negative layer charge produced was −1 per $O_{20}(OH)_4$. The partial hydration of divalent cations (Mg^{2+}, Ca^{2+}, Sr^{2+}, and Ba^{2+}) was studied using four hydration models: (1) a 'dry' model (no water molecules); (2) a one-water-layer model with four water molecules coordinated to the cation (4W_1L) in the interlayer space; (3) a one-water-layer model with six water molecules – two water molecules were added to model 2 (6W_1L); and (4) a two water-layer model with six water molecules octahedrally coordinating the cation (6W_2L). For comparison, the model with the monovalent cation (Na^+) in the interlayer space was also studied in which case only one isomorphic Al^{3+}/Mg^{2+} substitution was generated to produce the negative excess layer charge q = −0.5 per $O_{20}(OH)_4$. Four/six water molecules in the 1L and 2L models represent an ideal coordination in planar/octahedral cation complex and are also consistent, to a certain extent, with experimental observations (*e.g.* Ferrage *et al.*, 2005, 2007a). The number of interlayer water molecules in experimental works was considered as a variable parameter in fitting the experimental XRD patterns of samples in different hydration conditions and, therefore, varied with respect to the cation type and relative humidity. In the present study, the same number of water molecules was used for all cations studied in order to achieve consistent computational models.

Ab initio simulations

All calculations were performed using the Vienna *Ab Initio* Simulation Package, VASP (Kresse and Hafner, 1993; Kresse and Furthmüller, 1996), which is based on density functional theory (DFT). The parameterization of the local exchange-correlation function according to Perdew and Zunger (1981), together with a generalized gradient approximation (GGA) for non-local corrections (Perdew and Wang, 1992), was used. The Kohn-Sham equations were solved variationally with a plane-wave (PW) basis set using an energy cutoff of 400 eV in the projector-augmented-wave (PAW) method (Blöchl, 1994; Kresse and Joubert, 1999). Brillouin-zone sampling was restricted to the γ-point only because of the use of relatively large computational cells.

The study of different types of cations in the interlayer space and their hydration steps requires the user to find an optimal shape and volume for the unit cell. The dominant change in the cell volume during the hydration will clearly be related to the change in the c vector. Most studies of swelling of smectite minerals have been carried out with fixed a and b cell parameters where only the c vector or basal spacing (d_{001}) (perpendicular distance between layers = z component of the c vector) varied. In the present work the question of how all the cell parameters change during the volume expansion under the effect of hydration of the interlayer cations was tackled. For this purpose a certain interval of cell volumes for each model system was scanned. In practice, the c vector was varied by ~1 Å. For each point the full geometry relaxation of atomic positions and of volume shape (cell parameters) was performed, keeping the cell volume constant. The optimization procedure was based on a conjugate-gradient algorithm with a stopping criterion of 10^{-5} eV for the total energy, and of 0.01 eV/Å for the root mean square force. No symmetry restrictions were applied during any relaxation procedure. The number of points for each system was 10–12. The energy dependence with respect to the volume change was plotted. Formally, such a plot can be fitted with the third-order four parametric Birch-Murnaghan equation of state (BM-EOS) (Birch, 1947) to obtain information about a compliance/hardness of the studied structure. One parameter in the BM-EOS fit is the bulk modulus, B_0, a quantity reflecting the elastic behavior of the studied material as a response to external pressure. The fit of the BM-EOS is usually done with respect to a pressure-volume or energy-volume plot. In the latter case, the energy change is usually calculated with respect to the isostatic volume compression. Generally, bulk modulus is a second-order tensor for solids and in the case of anisotropic material such as clay minerals, its individual components can differ significantly. Note that in some cases in the calculations (especially on hydrated cations) some of the points of energy-volume data obtained did not fit ideally onto BM-EOF curves. Careful checking of the geometry of each point showed some small discontinuous changes in the geometry of interlayer species during the stepwise compression, *e.g.* re-switching of the hydrogen bonds of water molecules to neighboring oxygen atoms of the montmorillonite layer. This resulted in a deviation of some points from the ideal shape of the BM-EOF curve.

https://doi.org/10.1346/CCMN.2010.0580204 Published online by Cambridge University Press

RESULTS AND DISCUSSION

'Dry' montmorillonite

The structure of the dry montmorillonite system where the cation is 'sandwiched' between two layers (Figure 1) shows that the cation has a position in the middle between two layers and approximately above/below the center of the ditrigonal holes of two adjacent tetrahedral sheets. One of the parameters obtained from the fit of the BM-EOF to the energy-volume curve is the equilibrium volume, V_0, of the unit cell$_0$. The corresponding equilibrium lattice parameters were estimated from the plot of their dependence on the volume change (Figures 2, 3; both figures contain plots for different steps of cation hydration, discussed below). The *b* lattice vectors increase only slightly with volume expansion (Figure 2a). The monoclinic shape of the cell (Figure 3) was clearly preserved during the volume expansion as both the α and γ angles deviated only slightly from the ideal 90º value. The β angle decreased only slightly with volume expansion. Very similar trends in the dependence of the lattice parameters on the volume expansion have also been observed for all the studied divalent cations. The values of the cell parameters corresponding to the equilibrium volume, V_0, obtained for all the cations in dry state (Table 1) revealed that the calculated cell parameters *a*, *b*, α, β, and γ were almost unaffected by the type of interlayer cation. The calculated *a* and *b* vectors were only slightly larger than the experimental values from Tsipursky and Drits (1984). Hernández-Laguna *et al.* (2006) obtained larger *a* and *b* vectors (5.27−5.29 and 9.9−9.13 Å) for models similar to those in the present study ($Na^+/Mg^{2+}/Ca^{2+}$, octahedral substitution). Those authors also used the GGA but with a different parameterization (PBE, Perdew *et al.* 1996) compared to calculations in the present study. The

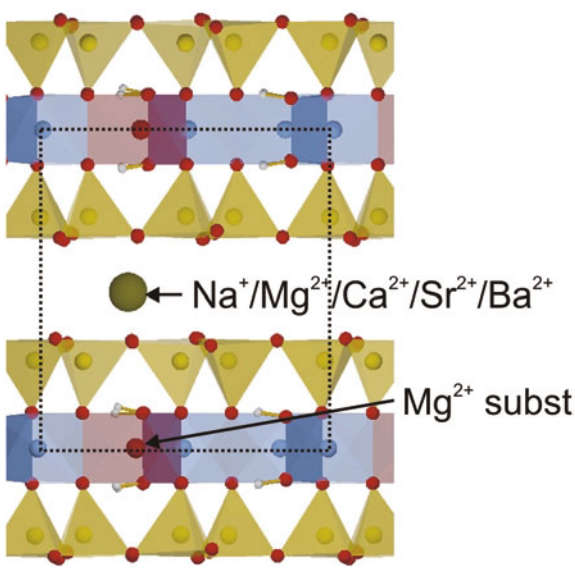

Figure 1. Model structure of dry montmorillonite. The clay layer is represented by the polyhedral model, the interlayer cation is represented by the ball style. The dashed rectangle represents the computational cell ($b \times c$).

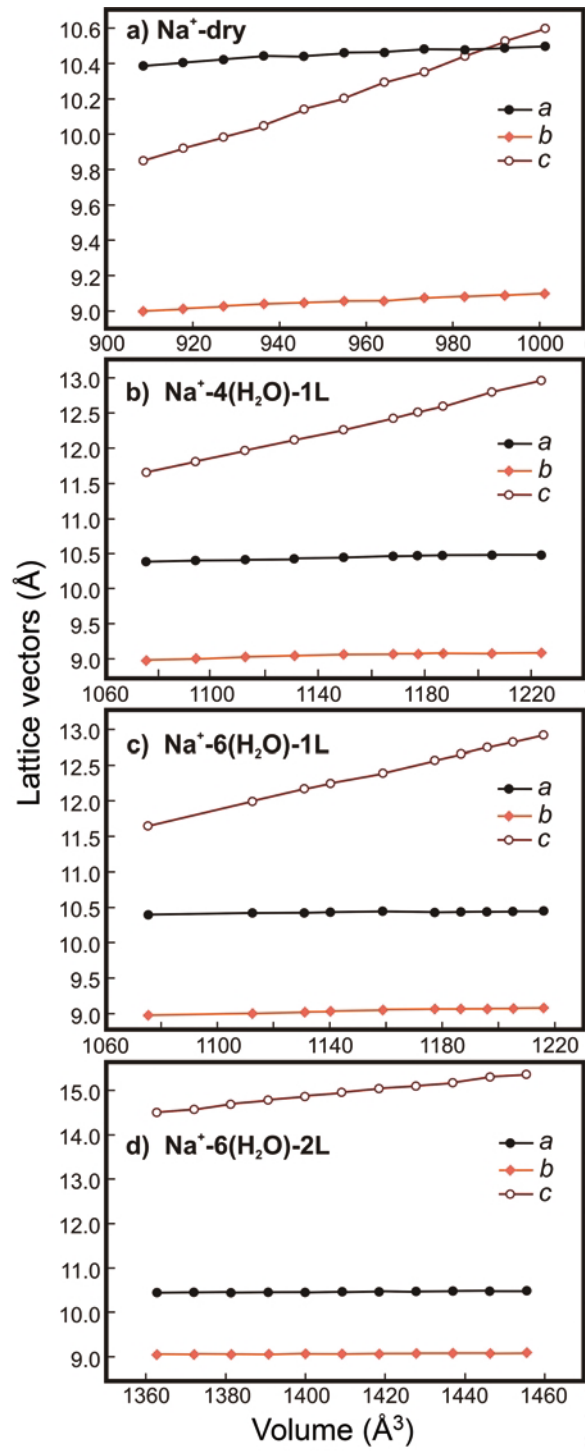

Figure 2. Optimized lattice vectors of Na^+-montmorillonite as a function of unit-cell volume.

https://doi.org/10.1346/CCMN.2010.0580204 Published online by Cambridge University Press

second difference was in the basis set used. While in the present study, plane waves were used, Perdew *et al.* (1996) used strictly localized numerical atomic orbitals. The β angles calculated here were ~99º and were somewhat smaller than the experimental values (99.5−101.4º) from Tsipursky and Drits (1984). On the other hand, Hernández-Laguna *et al.* (2006) obtained values of ~103º. In another theoretical work (Chatterjee *et al.*, 2004) on similar montmorillonite models (DFT method, plane-wave basis set, GGA approximation, Becke-Perdew parameterization (Perdew, 1986; Becke 1988)) smaller values for the calculated *a* and *b* cell vectors were obtained. Moreover, the *a* and *b* cell vectors calculated by Chatterjee *et al.* (2004) showed greater fluctuation with respect to the type of interlayer cation than in the present study or in the Hernández-Laguna *et al.* (2006) work. The β angles calculated are very similar to present results.

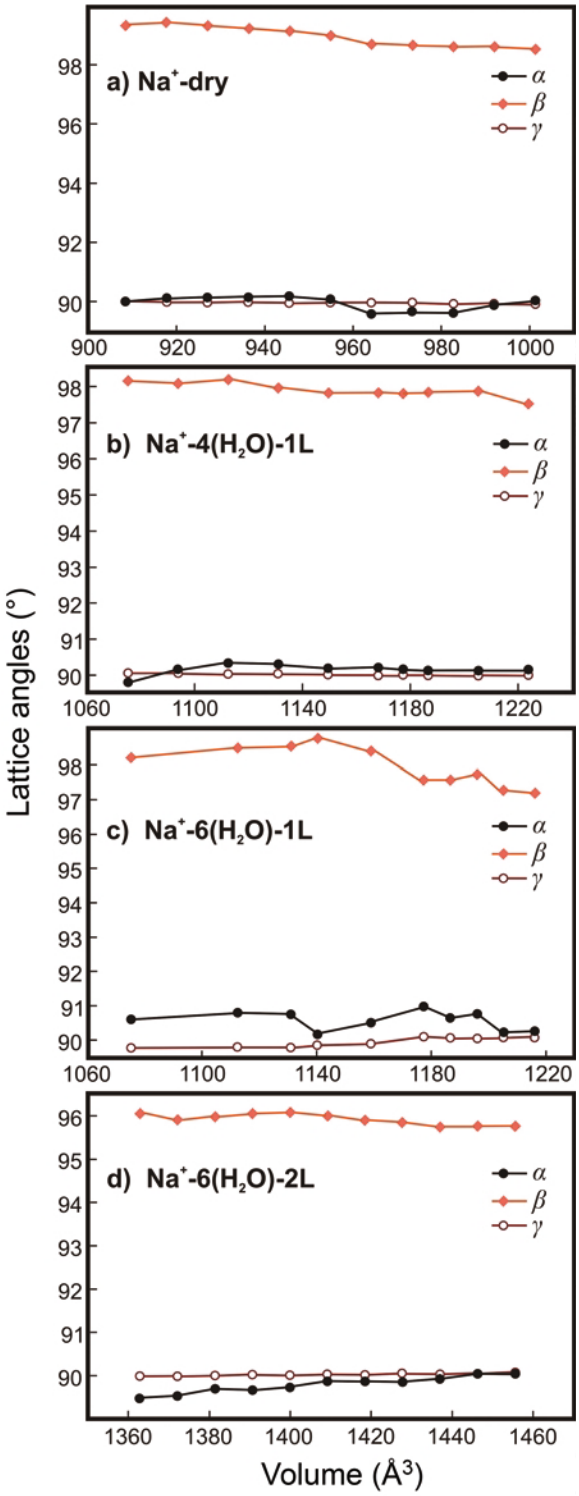

Figure 3. Optimized lattice angles of Na^+-montmorillonite as a function of unit-cell volume.

As expected, the interlayer cation had the greatest effect on the *c* vector and related *d* spacing. The largest *c* lattice vector from the set of cations studied was for the monovalent cation Na^+ (Table 1). All four structures with divalent cations had smaller *c* vectors than the Na^+-montmorillonite structure. Three (Mg^{2+}, Ca^{2+}, and Sr^{2+}) had very similar *c* vectors, close to ~10 Å, *i.e.* similar to the results of Hernández-Laguna *et al.* (2006). On the other hand, Chatterjee *et al.* (2004) reported larger *c* vectors than those obtained in the present study and a monotonic increase in *c* from the Mg^{2+}- to Ba^{2+}-exchanged structures, with no anomaly for the Ca^{2+}-exchanged structure as was observed here (Table 1). Surprisingly, the structure for the divalent cation with the largest ionic radius, Ba^{2+} (see Table 2), had a smaller *c* vector than the structure with the monovalent Na^+ cation; this can be explained by the larger Coulombic effect of the divalent cations than the monovalent cations, resulting in more compact layer stacking. Because of this finding, and coupled with the observed anomaly for the Ca^{2+} cation (smaller *c* vector than for the Mg^{2+} even though Ca^{2+} has a larger cationic radius), a greater emphasis was placed on the location of the cation in the interlayer space. Comparing results from the measured interatomic distances between the interlayer cation and the twelve oxygen atoms from the upper and lower ditrigonal holes packing the cation (Table 2), cations with smaller atomic radii (Mg^{2+}, Ca^{2+}, and Na^+) are clearly not located symmetrically above and below the approximate centers of the ditrigonal holes. Two sets (in the case of Mg^{2+}, three sets) of distances to oxygen atoms were found and the interlayer cations shifted from the center toward these oxygen atoms. Mg^{2+} has the shortest distance (~2.1 Å) to the four oxygen atoms (two from the upper and two from the lower ditrigonal hole), four intermediate distances (3.1−3.6 Å), and four distances >4.2 Å. Only cations with the largest ionic radius, Sr^{2+} and Ba^{2+}, were located close to the middle of the connection between the centers of the ditrigonal holes. The average cation−oxygen distance (Table 2) is, therefore, not a good parameter to explain the location of

https://doi.org/10.1346/CCMN.2010.0580204 Published online by Cambridge University Press

Table 1. Equilibrium cell volume, V_0, and corresponding cell parameters of the dry montmorillonite models obtained from the BM-EOF fit.

Cation	a (Å)[a]	B (Å)	c (Å)	α (°)	β (°)	γ (°)	V_0 (Å^3)
Exp.[b]	5.18	8.97–9.01	10.05–10.2	90.0	99.5–101.4	90.0	
Na^+	5.24	9.08	10.36	89.6	98.7	90.0	974.35
Mg^{2+}	5.25	9.03	10.07	90.7	99.2	89.7	942.83
Ca^{2+}	5.24	9.03	10.05	90.9	99.3	90.0	940.12
Sr^{2+}	5.24	9.06	10.06	90.0	99.2	90.0	943.14
Ba^{2+}	5.25	9.08	10.25	90.1	99.0	90.0	965.31

[a] computational cell with 2a lattice vector was used in calculations.
[b] Tsipursky and Drits (1984) (K-saturated smectites); Sato *et al.* (1992) (Na-montmorillonites).

the cation in the interlayer space as Na^+ and Mg^{2+} seem to have the largest values.

The calculated relative energy points with respect to the change of the z coordinate of the c vector (d_{001} spacing) and corresponding BM-EOF fit curves for all five cations were plotted (Figure 4). The estimated optimal d_{001} value from the BM-EOF fit (Table 3), together with the value of the bulk modulus, B_0, obtained from the fit to the calculated energy-volume points (recall that B_0 in this case represents the compliance of the clay structure with respect to the direction perpendicular to the montmorillonite layers because the a and b vectors changed only minimally during the cell-volume expansion/compression at low pressures) shows that the smallest B_0 value was obtained for the Na^+-montmorillonite compared to the structures with divalent cations, implying that the Na^+-montmorillonite is a more elastic material while all four structures with divalent cations are more compact due to the stronger Coulombic interactions. The results of calculated lattice parameters discussed above tie in with that observation. The stronger Coulombic field of the divalent cations forms more rigid structures than does the monovalent Na^+ cation. The calculated d_{001} values are in relatively good agreement with the available experimental data except for the Na^+ cation (Table 3). For 'dry' Na^+-montmorillonite, all available experimental data are more or less consistent in the determination of the d_{001} value ranging from 9.5 to 9.8 Å. The 10.17 Å result from calculations by Chatterjee *et al.* (2004), however, is similar to the present result (Table 3). One indication of the difference was that the pseudopotential used for the Na atom in the calculations was not adequate to describe the Na^+ cation. Two other Na atomic pseudopotentials, available in the program *VASP*, were therefore tested also. The results obtained were almost identical to those obtained using the original pseudopotential value. For hydrated states of Na^+, good agreement with experimental values was also obtained (see below). The question of why the experimental and calculated d_{001} values differs is, therefore, still unanswered. Experimental determination of d_{001} does have limited accuracy. d_{001} is entered as a parameter to fitting of experimental XRD patterns of samples in which various proportions of 0, 1, and 2 water layers exist, and the ratio of these proportions is affected by experimental conditions, *e.g.* relative humidity (Ferrage *et al.*, 2005, 2007a).

Hydrated one-water-layer montmorillonites (four and six water molecules)

A montmorillonite model structure with an interlayer cation coordinated by four water molecules which are located approximately in one plane (one-layer model – 1L), is shown in Figure 5. The cation in the planar complex has an axial coordination by basal oxygen atoms surrounding a ditrigonal hole in the upper and lower layers. The structures with interlayer complexes of all five cations were optimized in the same manner as in

Table 2. Calculated cation–O_{basal} distances in dry montmorillonite structures at equilibrium unit-cell volume, V_0. A, B, and C are three different intervals; the numbers in parenthesis are the number of basal oxygen atoms from the upper and lower montmorillonite layers. R_{cat} is the Pauling cation radius. All numbers are in Å.

Cation	A	B	C	Average	R_{cat}
Na^+	2.4–3.1 (6)	–	3.5–3.9 (6)	3.22	0.95
Mg^{2+}	~2.1 (4)	3.1–3.6 (4)	4.2–4.5 (4)	3.25	0.65
Ca^{2+}	2.5–3.1 (6)	–	3.3–3.8 (6)	3.07	0.99
Sr^{2+}	~2.9 (6)	–	~3.1 (6)	3.03	1.13
Ba^{2+}	~3.0 (6)	–	3.1–3.2 (6)	3.09	1.35

https://doi.org/10.1346/CCMN.2010.0580204 Published online by Cambridge University Press

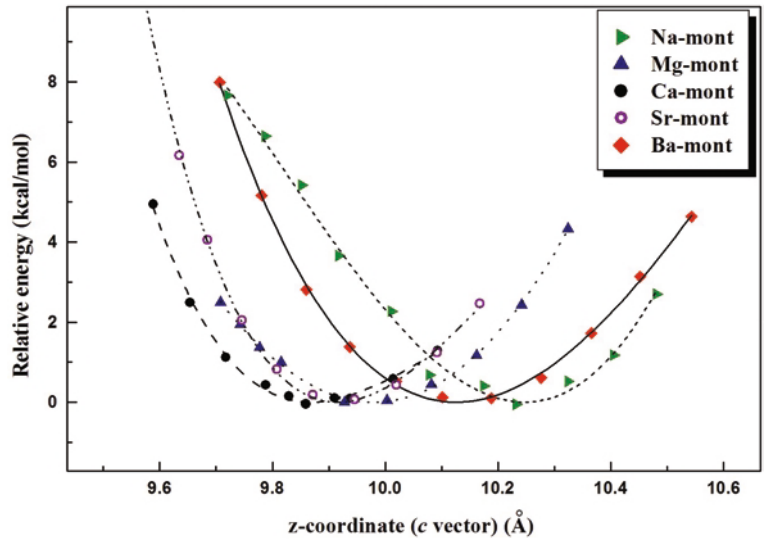

Figure 4. Final relative energy as a function of basal spacing for the dry (Na^+/Mg^{2+}/Ca^{2+}/Sr^{2+}/Ba^{2+})-exchanged montmorillonite. Computed data are fitted to the 2nd order Birch-Murnaghan equation of state.

Table 3. Calculated basal spacing, d_{001} (Å), and bulk modulus, B_0, for studied montmorillonite models. d_{001} values are compared with results collected from the literature.

M-montmorillonite	Theory		Experiment	B_0 (Mbar)
	This work	Chatterjee *et al.* (2004)[a]		
Na^+-dry	10.24	10.17	9.55[b,c], 9.6[d], 9.60[e], 9.83[f]	0.13±0.01
Na^+-4(H_2O)-1L	12.43	11.51	12.5[b,c], 12.7[d], 12.3–12.55[e], 12.57[g]	0.11±0.02
Na^+-6(H_2O)-1L	12.53			0.12±0.02
Na^+-6(H_2O)-2L	14.93		15.55[b,c], 15.55[e]	0.11±0.01
Mg^{2+}-dry	9.94	9.81	9.6[d], 10.0[e], 10.0f	0.22±0.04
Mg^{2+}-4(H_2O)-1L	11.66	10.34	11.5–13.00[e], 12.1f	0.25±0.01
Mg^{2+}-6(H_2O)-1L	12.59			0.06±0.02
Mg^{2+}-6(H_2O)-2L	14.37		15.1[d], 14.0–15.9f	0.09±0.01
Ca^{2+}-dry	9.93	9.98	9.6[d], 10.00[e], 9.55[f], 9.55–9.7[h], 10.3[i]	0.25±0.03
Ca^{2+}-4(H_2O)-1L	11.96	11.33	11.65–12.85[e], 12.07–12.50[f], 11.7[i], 11.19–12.45[j]	0.18±0.01
Ca^{2+}-6(H_2O)-1L	12.31			0.12±0.01
Ca^{2+}-6(H_2O)-2L	14.72		15.0[d], 14.30–15.51[e], 15.15–15.6[f], 15[i,k], 15.24–15.81[j]	0.11±0.01
Sr^{2+}-dry	9.93	10.11	9.9[d], 9.80–10.00[e], 9.64f	0.24±0.00
Sr^{2+}-4(H_2O)-1L	12.07	10.63	11.90–12.70[e], 12.1–12.25[f]	0.18±0.01
Sr^{2+}-6(H_2O)-1L	12.44			0.13±0.01
Sr^{2+}-6(H_2O)-2L	14.92		14.4[d], 15.10–15.73[e] 15.26–15.79f	0.10±0.01
Ba^{2+}-dry	10.12	10.39	11.3[d], 9.85[f]	0.21±0.00
Ba^{2+}-4(H_2O)-1L	12.20	11.10	12.4[d], 12.0–12.3[f]	0.19±0.01
Ba^{2+}-6(H_2O)-1L	12.72			0.16±0.01
Ba^{2+}-6(H_2O)-2L	15.15		15.9–16.1d	0.09±0.03

[a] DFT results only, Chatterjee *et al.* (2004); for hydrated samples only a 1L model was considered.
[b] Cuadros (1997)
[c] Bérend *et al.* (1995)
[d] Abramova *et al.* (2007); dry samples were treated at 375ºC; for hydrated samples the type of water layer was not specified.
[e] Ferrage *et al.* (2005)
[f] Cases *et al.* (1997)
[g] Fu *et al.* (1999)
[h] Rutherford *et al.* (1997)
[i] Bray *et al.* (1998)
[j] Sato *et al.* (1992)

https://doi.org/10.1346/CCMN.2010.0580204 Published online by Cambridge University Press

case of the 'dry' structures. Later the structures with four water molecules were modified by adding two additional water molecules to the interlayer space. The structures with six water molecules were again optimized. The two additional molecules did not penetrate directly into the coordination sphere of the cation but were located close to the original four water molecules (Figure 6). The one-water-layer structures with four and six water molecules were expanded/compressed with small steps in volume change in the same way as was done for the 'dry' structures. From the fit of the BM-EOF to the energy-volume curve, the optimal cell parameters and volume were obtained. A plot of the relative energy with respect to the change in the z coordinate for all five cations (Figure 7) revealed that changes in lattice parameters (vectors and angles) with respect to the volume change have a trend very similar to that described for the 'dry' structures (Figures 2b,c, 3b,c for Na^+-montmorillonite 1L models) meaning that the lattice vectors a and b and also the cell angles change only slightly. The largest cell-volume change is related to the change in the c vector. From the BM-EOF fit, the equilibrium cell volume, V_0, and cell parameters were estimated (Table 4) for the corresponding d_{001} values (Table 3). The formation of hydrated montmorillonite structures with a one-layer arrangement results in the expansion of the interlayer space with the extension of the d_{001} parameter from ~10 Å ('dry') to ~12 Å and more (Table 3). The d_{001} values calculated here are in good agreement with available experimental values (see data in Table 3). The d_{001} values calculated by Chatterjee *et al.* (2004) are smaller than in the present case, probably because of an overestimated Coulombic effect in the Chatterjee models – they used a unit cell which is half of the computational cell used in the present study. Also, values for mutual interactions among cation-water complexes in neighboring computational cells were greater in the Chatterjee study than in the present calculations.

The planar cation complexes are relatively regular where the cation is not centered above the ditrigonal hole but the whole complex is shifted in such a way that two basal oxygen atoms from the upper and lower ditrigonal holes completed the six-coordination of the cation. The final position of the planar complex is also ruled by the effective formation of the hydrogen bonds between water molecules and the basal oxygen atoms of the montmorillonite layer. The distances of the cation to the basal oxygen atoms in the coordination sphere and the lengths of the hydrogen bonds dictate the final d_{001} spacing. In the case of divalent cations, the distances between water ligand and cation increase regularly with increasing ionic radius and are: 2.0–2.2 Å for Mg^{2+}, 2.3–2.4 Å for Ca^{2+}, 2.5 Å for Sr^{2+}, and 2.7 Å for Ba^{2+}. The axial distances between the cation and the basal oxygen atoms are greater than the distances in the

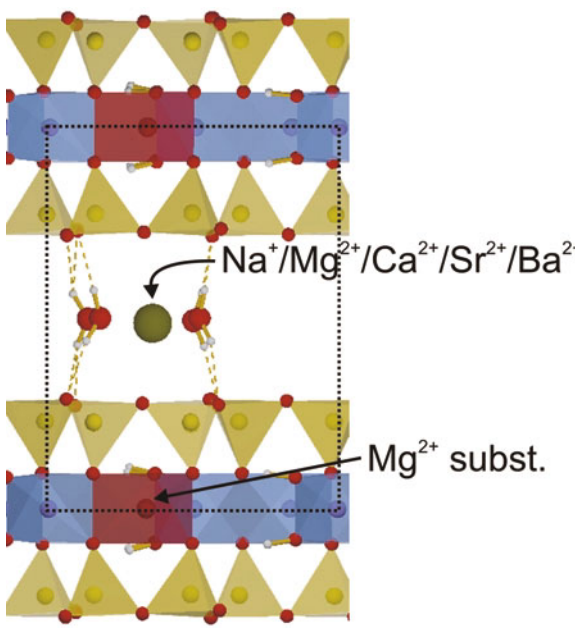

Figure 5. Model structure of 1-layer montmorillonite hydrate with four water molecules. The clay layer is represented by a polyhedral model; the interlayer cation is represented by the ball style. The dashed rectangle represents the computational cell ($b \times c$).

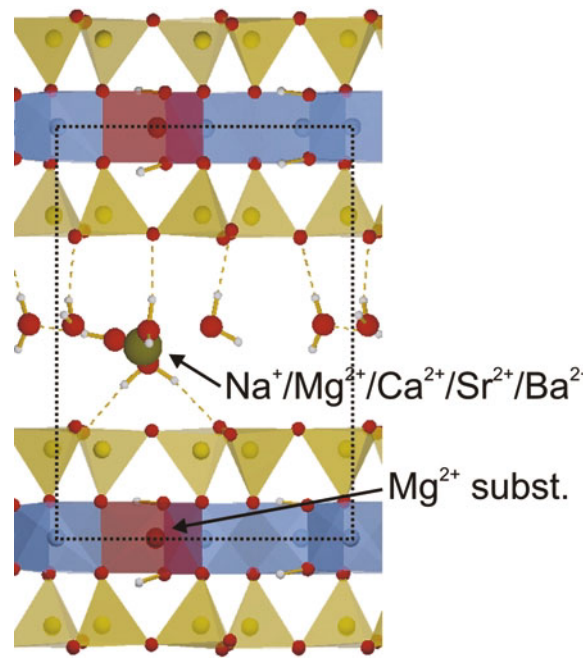

Figure 6. Model structure of 1-layer montmorillonite hydrate with six water molecules. The clay layer is represented by the polyhedral model; the interlayer cation is represented by the ball style. The dashed rectangle represents the computational cell ($b \times c$).

https://doi.org/10.1346/CCMN.2010.0580204 Published online by Cambridge University Press

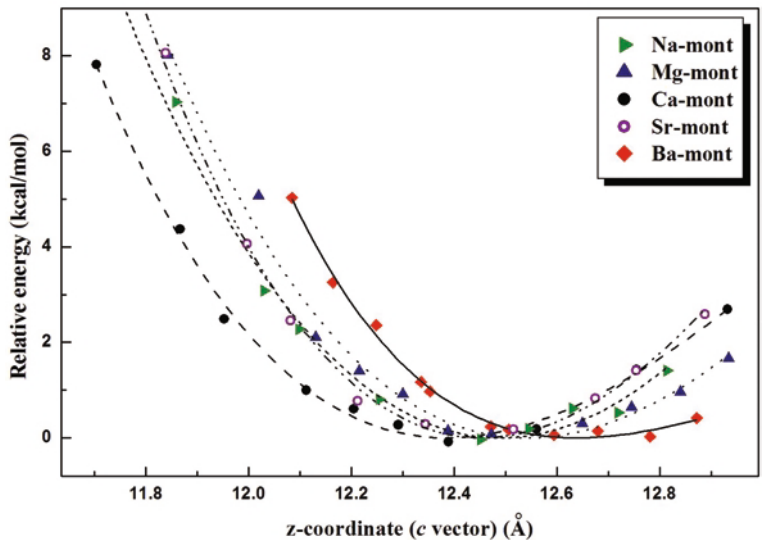

Figure 7. Final relative energy as a function of basal spacing for 1-layer (Na^+/Mg^{2+}/Ca^{2+}/Sr^{2+}/Ba^{2+})-exchanged montmorillonite hydrate with six water molecules. Computed data are fitted to the 2nd order Birch-Murnaghan equation of state.

equatorial plane and regularly increase for increasing cation radius (*e.g.* 2.35 Å for Mg^{2+}, 2.95 Å for Ba^{2+}). The type of cation also affects the length of the hydrogen bonds formed between the water molecules and the basal oxygen atoms. The smaller cation has the larger polarization effect on the water ligand resulting in shorter hydrogen bonds. For example, the H···O_b distances are ~1.8−1.9 Å for Mg^{2+} and 2.1−2.2 Å for Ba^{2+}. The monovalent Na^+ cation has a smaller ligand and polarization effect than divalent cations, and therefore the d_{001} spacing obtained is greater than in the case of the largest divalent cation Ba^{2+} (Table 3). The distances between Na^+ and water oxygen atoms are ~2.4 Å and hydrogen-bond lengths are ~2.1−2.4 Å.

The presence of two additional water molecules (1L models with six H_2O) resulted in the extra expansion of d_{001} by ~0.1−0.5 Å except for Mg^{2+} (~1 Å) (Table 3). The two additional water molecules form hydrogen bonds with the basal oxygen atoms and also interact with the water molecules in the first coordination shell of the interlayer cation resulting in perturbation of the planarity of the interlayer complex, especially for extended volumes. The interatomic distances between the cation and the oxygen atoms in the planar complex do not change significantly in comparison with the 1L model with four water molecules.

With the next extension of volume, the two extra water molecules will have the tendency to enter into the first coordination sphere of the interlayer cation to form a six-coordinated complex with the water molecules arranged in a so-called 'two-water-layer model' (2L, discussed below). The calculated bulk modulus values, B_0 (Table 3), are smaller than corresponding data obtained for the 'dry' structures, meaning that water

Table 4. Equilibrium cell volume, V_0, and corresponding cell parameters of the hydrated one-water-layer montmorillonite models with four and six water molecules obtained from the BM-EOF fit.

Cation	*a* (Å)[a]	*b* (Å)	*c* (Å)	α	β (º)	γ (º)	V_0 (Å^3)
Na^+-4W	5.23	9.08	12.55	90.1	97.8	90.0	1182.15
Na^+-6W	5.22	9.08	12.64	90.7	97.7	90.0	1185.92
Mg^{2+}-4W	5.23	9.05	11.76	90.1	97.5	89.9	1102.75
Mg^{2+}-6W	5.24	9.06	12.70	90.2	97.4	89.8	1193.19
Ca^{2+}-4W	5.23	9.04	12.07	90.2	97.7	90.0	1128.86
Ca^{2+}-6W	5.23	9.02	12.42	90.1	97.8	90.1	1168.72
Sr^{2+}-4W	5.25	9.09	12.19	90.3	98.2	90.0	1152.53
Sr^{2+}-6W	5.24	9.08	12.57	90.5	98.3	90.0	1183.12
Ba^{2+}-4W	5.23	9.03	12.32	90.2	97.9	90.0	1154.39
Ba^{2+}-6W	5.23	9.04	12.83	90.3	97.5	90.0	1200.48

[a] A computational cell with a 2*a* lattice vector was used in the calculations.

https://doi.org/10.1346/CCMN.2010.0580204 Published online by Cambridge University Press

molecules in the interlayer space caused a certain softening of the hydrated montmorillonites. Such a tendency is more significant for divalent cations than for a monovalent Na^+ cation, implying that the type of cation in the interlayer space of montmorillonites has a significant effect on the mechanical properties of the clay minerals.

Hydrated two-water-layer montmorillonites

A hydrated cation complex in a 2L montmorillonite model has octahedral coordination and is located in the interlayer space in such a way that three water molecules are close to the lower montmorillonite layer while the other three water molecules are close to the upper layer (Figure 8). The relative energy dependence on the volume change for all five cations is shown in Figure 9. The equilibrium volume of the unit cell, V_0, and corresponding cell parameters are collected in Table 5. The variations in the lattice parameters with respect to the volume change are very similar to those observed for the 'dry' and 1L structures (compare Figures 2d and 3d for the Na^+-montmorillonite 2L model). The extension of the d_{001} spacing with increasing ionic radius is observed for the divalent cations and the calculated results fit very well with the experimental data available (Table 3). The cell expansion also correlates with the increasing cation–oxygen distances in the cation hexaaquo complex and the hydrogen bonds formed between the water molecules and the basal oxygen atoms. The calculated cation–oxygen interatomic distances are 2.03–2.15 Å for Mg^{2+}, 2.32–2.40 Å for Ca^{2+}, 2.52–2.55 for Sr^{2+}, and 2.70–2.75 Å for Ba^{2+}. The strong polarization effect of the divalent cations on water molecules results in the relatively short (1.7 to 1.9 Å) hydrogen bonds between hydrogen atoms of water molecules and the basal oxygen atoms. The hydrogen bonds are a little shorter than those observed for the 1L hydrated montmorillonite models with

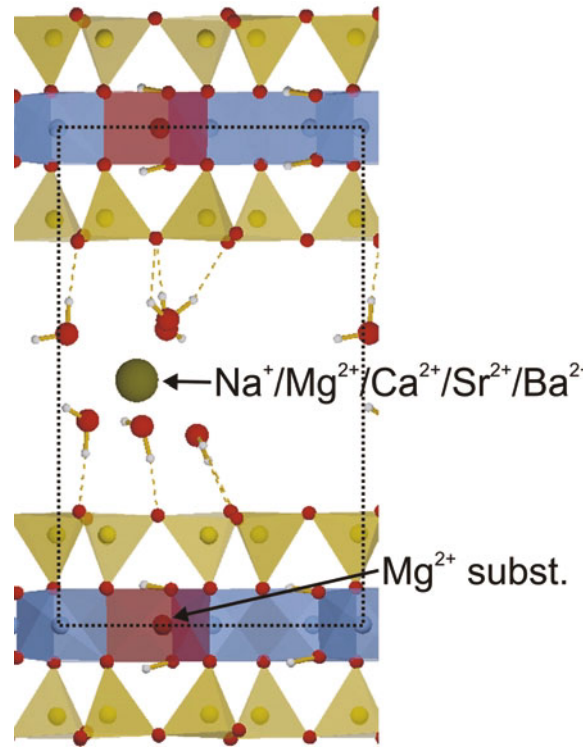

Figure 8. Model structure of 2-layer montmorillonite hydrate with six water molecules. The clay layer is represented by the polyhedral model; the interlayer cation is represented by the ball style. The dashed rectangle represents the computational cell ($b \times c$).

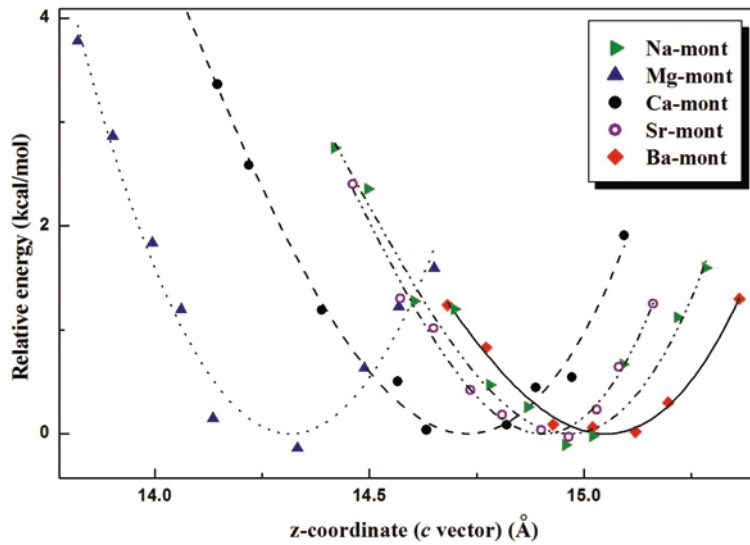

Figure 9. Final relative energy as a function of basal spacing for 2-layers ($Na^+/Mg^{2+}/Ca^{2+}/Sr^{2+}/Ba^{2+}$)-exchanged montmorillonite hydrate, six water molecules. Computed data are fitted to the 2nd order Birch-Murnaghan equation of state.

https://doi.org/10.1346/CCMN.2010.0580204 Published online by Cambridge University Press

Table 5. Equilibrium cell volume, V_0, and corresponding cell parameters of the two-water-layer montmorillonite models obtained from the BM-EOF fit.

Cation	a (Å)[a]	b (Å)	c (Å)	α (º)	β (º)	γ (º)	V_0 (Å)^3
Na^+	5.23	9.06	15.02	89.9	96.0	90.0	1415.50
Mg^{2+}	5.22	9.04	14.45	90.2	96.1	90.0	1357.11
Ca^{2+}	5.22	9.04	14.80	90.1	96.0	90.0	1388.81
Sr^{2+}	5.25	9.08	15.01	89.9	96.1	90.0	1423.49
Ba^{2+}	5.23	9.04	15.23	90.0	95.9	90.0	1430.86

[a] A computational cell with a 2a lattice vector was used in the calculations.

divalent cations. The 2L montmorillonite model with Na^+ has a relatively large d_{001} value – similar to the models with large divalent cations (Sr^{2+} and Ba^{2+}). The reason is the smaller polarization effect of the Na^+ cation in comparison with those of divalent cations. The Na^+–oxygen distances in the optimal structure are 2.4–2.6 Å and the hydrogen bond lengths are ~1.9–2.1 Å.

Values obtained for the calculated bulk modulus, B_0, were smaller than for 1L models (Table 3), implying increasing elasticity of the hydrated material. Only small differences in B_0 values were observed for different cations such that at greater degrees of hydration of the montmorillonite structures, the nature of the cations was less important than in case of the 'dry' structures. The B_0 values obtained showed that the water content became the dominant factor for elastic properties of hydrated montmorillonite phases.

CONCLUSIONS

A theoretical study of the hydration properties of homoionic montmorillonite systems containing divalent cations in the interlayer space was carried out. For comparison, the monovalent structure (Na^+ cation) was also studied. First-principles calculations based on density functional theory (DFT) were performed on the set of models with different levels of cation hydration: (1) 'dry;' (2) one-layer model with four water molecules; (3) one-water-layer model with six water molecules; and (4) two-water-layer model with six water molecules. The dry structures with divalent cations were found to have more compact and rigid structures than structures with monovalent cations as demonstrated by the calculation of the bulk modulus, B_0, using the Birch-Murnaghan equation of states. The d_{001} values did not change regularly with increasing ionic radius in the dry structures; this was assigned to the slightly different locations of the cation in the space between the ditrigonal holes of the tetrahedral sheet. Smaller cations (Mg^{2+}, Ca^{2+}) are preferentially located close to some of the basal oxygen atoms of the ditrigonal holes, while larger cations (Sr^{2+}, Ba^{2+}) are located relatively symmetrically above and below the ditrigonal holes. The calculated d_{001} values were in relatively good agreement with experimental values; a discrepancy was observed only for the Na^+ cation.

One-layer hydration results in the expansion of the interlayer space and calculated d_{001} parameters are in good agreement with values presented in the literature for one-water-layer montmorillonite structures. The models with divalent cations were, again, more compact than structures with monovalent cations. Computed d_{001} spacing values reflect the nature of the hydrated cation – with increasing ionic radius, the cation–oxygen distances in the interlayer complex increase resulting in increased d_{001} values. The type of cation also affects the hydrogen bonds formed between the water molecules and the basal oxygen atoms of the montmorillonite layers. The largest interlayer expansion was observed for two-water-layer models with octahedrally coordinated interlayer cations. The interlayer space increased regularly with increasing ionic radius of the divalent cation correlating with the measured cation–oxygen distances in the hexaquo complex.

The calculated B_0 parameters for hydrated models are significantly smaller than for dry structures such that hydrated montmorillonites are more elastic than dry ones. For greater degrees of hydration (2L model) the calculated bulk modulus was observed to be less dependent on the type of interlayer cation; in hydrated montmorillonites, compliance of the material is, therefore, mainly dictated by the hydrogen bonds formed between the water molecules and the montmorillonite layers.

ACKNOWLEDGMENTS

DT thanks the German Research Foundation, priority program SPP 1315, project No. GE 1676/1-1 for support of this work.

REFERENCES

Abramova, E., Lapides I., and Yariv, S. (2007) Thermo-XRD investigation of monoionic montmorillonites mechano-chemically treated with urea. *Journal of Thermal Analysis and Calorimetry*, **90**, 99–106.

Bailey, S.W. (editor) (1988) *Hydrous Phyllosilicates (Exclusive*

of Micas). Reviews in Mineralogy, **19**, Mineralogical Society of America, Washington, D.C., 725 pp.

Bains, A.S., Boek, E.S., Coveney, P.V., Williams, S.J., and Akbar, M.V. (2001) Molecular modelling of the mechanism of action of organic clay-swelling inhibitors. *Molecular Simulation*, **26**, 101–145.

Becke, A.D. (1988) Density-functional exchange-energy approximation with correct asymptotic behavior. *Physical Review A*, **38**, 3098–3100.

Bérend, I., Cases, J.-M., Francois, M., Uriot, J.-P., Michot, L., Masion, A., and Thomas, F. (1995) Mechanism of adsorption and desorption of water vapor by homoionic montmorillonites; 2, The Li^+, Na^+, K^+, Rb^+ and Cs^+-exchanged forms. *Clays and Clay Minerals*, **43**, 324–336.

Birch, F. (1947) Finite elastic strain of cubic crystals. *Physical Review*, **71**, 809–824.

Blöchl, P.E. (1994) Projector augmented-wave method. *Physical Review B*, **50**, 17953–17979.

Boek, E.S. and Sprik, M. (2003) Ab initio molecular dynamics study of the hydration of a sodium smectite clay. *The Journal of Physical Chemistry B*, **107**, 3251–3256.

Boek, E.S., Coveney, P.V., and Skipper, N.T. (1995) Monte Carlo molecular modeling studies of hydrated Li-, Na-, and K-Smectites: Understanding the role of potassium as a clay swelling inhibitor. *Journal of the American Chemical Society*, **117**, 12608–12617.

Botella, V., Timon, V., Escamilla-Roa, E., Hernandez-Laguna, A., and Sainz-Díaz, C.I. (2004) Hydrogen bonding and vibrational properties of hydroxy groups in the crystal lattice of dioctahedral clay minerals by means of first principles calculations. *Physics and Chemistry of Minerals*, **31**, 475–486.

Bray, H.J. and Redfern, S.A.T. (1999) Kinetics of dehydration of Ca-montmorillonite. *Physics and Chemistry of Minerals*, **26**, 591–600.

Bray, H.J. and Redfern, S.A.T. (2000) Influence of counterion species on the dehydroxylation of Ca^{2+}-, Mg^{2+}-, Na^+- and K^+-exchanged Wyoming montmorillonite. *Mineralogical Magazine*, **64**, 337–346.

Bray, H.J., Redfern, S.A.T., and Clark, S.M. (1998) The kinetics of dehydration in Ca-montmorillonite; an in situ X-ray diffraction study. *Mineralogical Magazine*, **62**, 647–656.

Cases, J.-M., Bérend, I., Francois, M., Uriot, J.-P., Michot, L.J., and Thomas, F. (1997) Mechanism of adsorption and desorption of water vapor by homoionic montmorillonite. 3. The Mg^{2+}, Ca^{2+}, Sr^{2+} and Ba^{3+} exchanged forms. *Clays and Clay Minerals*, **45**, 8–22.

Chang, F.R.C., Skipper, N.T., and Sposito, G. (1995) Computer-simulation of interlayer molecular-structure in sodium montmorillonite hydrates. *Langmuir*, **11**, 2734–2741.

Chatterjee, A. (2005) Application of localized reactivity index in combination with periodic DFT calculation to rationalize the swelling mechanism of clay type inorganic material. *Journal of Chemical Sciences*, **117**, 533–539.

Chatterjee, A., Ebina, T., Onodera, Y., and Mizukami, F. (2004) Effect of exchangeable cation on the swelling property of 2:1 dioctahedral smectite – a periodic first principle study. *The Journal of Chemical Physics*, **120**, 3414–3424.

Chávez-Páez, M., Van Workum, K., de Pablo, L., and de Pablo, J.J. (2001a) Monte Carlo simulations of Wyoming sodium montmorillonite hydrates. *The Journal of Chemical Physics*, **114**, 1405–1413.

Chávez-Páez, M., de Pablo, L., and de Pablo, J.J. (2001b) Monte Carlo simulations of Ca-montmorillonite hydrates. *The Journal of Chemical Physics*, **114**, 10948–10953.

Cuadros, J. (1997) Interlayer cation effects on the hydration state of smectite. *American Journal of Science*, **297**, 829–841.

Dios Cancela, G., Huertas, F.G., Romero Taboada, E., Sánchez-Rasero, F., and Hernández Laguna, A. (1997) Adsorption of water vapor by homoionic montmorillonites. Heats of adsorption and desorption. *Journal of Colloid and Interface Science*, **185**, 343–354.

Drits, V.A. (2003) Structural and chemical heterogeneity of layer silicates and clay minerals. *Clay Minerals*, **38**, 403–432.

Fang, Q.H., Huang, S.P., Liu Z.P., and Wang, W.C. (2004) Molecular dynamics simulation of magnesium-montmorillonite hydrates. *Acta Chimica Sinica*, **62**, 2407–2414.

Ferrage, E., Lanson, B., Sakharov, B.A., and Drits, V.A. (2005) Investigation of smectite hydration properties by modeling of X-ray diffraction profiles. Part 1. Montmorillonite hydration properties. *American Mineralogist*, **90**, 1358–1374.

Ferrage, E., Lanson, B., Sakharov, B.A., Geoffroy, N., Jacquot, E., and Drits, V.A. (2007a) Investigation of dioctahedral smectite hydration properties by modeling of X-ray diffraction profiles: Influence of layer charge and charge location. *American Mineralogist*, **92**, 1731–1743.

Ferrage, E., Kirk, C.A., Cressey, G., and Cuadros, J. (2007b) Dehydration of Ca-montmorillonite at the crystal scale. Part I: Structure evolution. *American Mineralogist*, **92**, 994–1006.

Fu, M.H., Zhang, Z.Z., and Low, P.F. (1990) Changes in the properties of a montmorillonite-water system during the adsorption and desorption of water: hysteresis. *Clays and Clay Minerals*, **38**, 485–492.

Giese, R.F. and van Oss, C.J. (2002) *Colloid and Surface Properties of Clays and Related Minerals*. Surfactant Science Series, **105**. Marcel Dekker, New York.

Greathouse J.A. and Storm, E.W. (2002) Calcium hydration on montmorillonite clay surfaces studied by Monte Carlo simulation. *Molecular Simulation*, **28**, 633–647.

Greathouse, J.A., Refson, K., and Sposito, G. (2000) Molecular dynamics simulation of water mobility in magnesium-smectite hydrates. *Journal of the American Chemical Society*, **122**, 11459–11464.

Guindy, N.M., El-Akkad, T.M., Flex, N.S., El-Massry, S.R., and Nashed, S. (1985) Thermal dehydration of mono- and di-valent montmorillonite cationic derivatives. *Thermochimica Acta*, **88**, 369–378.

Hernández-Laguna, A., Escamilla-Roa, E., Timón, V., Dove, M.T., and Sainz-Díaz, C.I. (2006) DFT study of the cation arrangements in the octahedral and tetrahedral sheets of dioctahedral 2:1 phyllosilicates. *Physics and Chemistry of Minerals*, **33**, 655–666.

Kantam, M.L., Choudary, B.M., Reddy, C.V., Rao, K.K., and Figueras, F. (1998) Aldol and Knoevenagel condensations catalysed by modified Mg-Al hydrotalcite: a solid base as catalyst useful in synthetic organic chemistry. *Chemical Communications*, 1033–1034.

Kato, M. and Usuki, A. (2000) Polymer-clay nanocomposites. Pp. 6–12 in: *Polymer-Layered Silicate Nanocomposites* (T.J. Pinnavaia and G.W. Beall, editors). Wiley, New York.

Keren, R. and Shainberg, I. (1975) Water vapor isotherms and heat of immersion of Na/Ca-montmorillonite systems; I. Homoionic clay. *Clays and Clay Minerals*, **23**, 193–200.

Kosakowski, G., Churakov, S.V., and Thoenen, T. (2008) Diffusion of Na and Cs in montmorillonite. *Clays and Clay Minerals*, **56**, 190–206.

Kresse, G. and Furthmüller, J. (1996) Efficiency of ab-initio total energy calculations for metals and semiconductors using a plane-wave basis set. *Computational Materials Science*, **6**, 15–50.

Kresse, G. and Hafner, J. (1993) Ab initio molecular dynamics

for open-shell transition metals. *Physical Review B*, **48**, 13115–13118.

Kresse, G. and Joubert, D. (1999) From ultrasoft pseudopotentials to the projector augmented-wave method. *Physical Review B*, **59**, 1758–1775.

Liu, Z., Chen, K., and Yan, D. (2003) Crystallization, morphology, and dynamic mechanical properties of poly (trimethylene terephthalate)/clay nanocomposites. *European Polymer Journal*, **39**, 2359–2366.

Majumdar, D., Blanton, T.N., and Schwark, D.W. (2003) Clay-polymer nanocomposite coatings for imaging application. *Applied Clay Science*, **23**, 265–273.

Manceau, A., Lanson, B., Drits, V.A., Chateigner, D., Gates, W.P., Wu, J., Huo, D., and Stucki, J.W. (2000) Oxidation-reduction mechanism of iron in dioctahedral smectites: I. Crystal chemistry of oxidized reference nontronites. *American Mineralogist*, **85**, 133–152.

Manju, G.N., Gigi, M.C., and Anirudhan, T.S. (1999) Hydrotalcite as adsorbent for the removal of chromium (VI) from aqueous media: equilibrium studies. *Indian Journal of Chemical Technology*, **6**, 134.

Marry, V., Turq, P., Cartailler, T., and Levesque, D. (2002) Microscopic simulation of structure and dynamics of water and counterions in a monohydrated montmorillonite. *Journal of Chemical Physics*, **117**, 3454–3463.

McEwan, D.M.C. and Wilson, M.J. (1980) Interlayer and intercalation complexes of clay minerals. Pp. 197–248 in: *Crystal Structures of Clay Minerals and their X-ray Identification* (G.W. Brindley and G. Brown, editors). Mineralogical Society, London.

Meleshyn, A. and Bunnenberg, C. (2005) Swelling of Na/Mg-montmorillonites and hydration of interlayer cations: A Monte Carlo study. *The Journal of Chemical Physics*, **123**, 074706.

Minisini, B. and Tsobnang, F. (2005) Ab initio comparative study of montmorillonite structural models. *Applied Surface Science*, **242**, 21–28.

Odriozola, G. and Aguilar, J.F. (2005) Stability of Ca-montmorillonite hydrates: A computer simulation study. *The Journal of Chemical Physics*, **123**, 174708.

Odriozola, G. and Guevara-Rodríguez, F. de J. (2004) Na-montmorillonite hydrates under basin conditions: Hybrid Monte Carlo and molecular dynamics simulations. *Langmuir*, **20**, 2010–2016.

Park, S.-H. and Sposito, G. (2000) Monte Carlo simulation of total radial distribution functions for interlayer water in Li-, Na-, and K-montmorillonite hydrates. *The Journal of Physical Chemistry B*, **104**, 4642–4648.

Perdew, J.P. (1986) Density-functional approximation for the correlation energy of the inhomogeneous electron gas. *Physical Review B*, **33**, 8822–8824.

Perdew, J.P. and Wang, Y. (1992) Accurate and simple analytic representation of the electron-gas correlation energy. *Physical Review B*, **45**, 13244–13249.

Perdew, J.P. and Zunger, A. (1981) Self-interaction correction to density-functional approximations for many-electron systems. *Physical Review B*, **23**, 5048–5079.

Perdew, J.P., Burke, K., and Ernzerhof, M. (1996) Generalized gradient approximation made simple. *Physical Review Letters*, **77**, 3865–3868.

Perkins, D. (1998) *Mineralogy: Upper Saddle River*. Prentice Hall, New Jersey.

Posner, A.M. and Quirk, J.P. (1964) Changes in basal spacing of montmorillonite in electrolyte solutions. *Journal of Colloid Science*, **19**, 798–812.

Qin, H., Su, Q., Zhang, S., Zhao, B., and Yang, M. (2003) Thermal stability and flammability of polyamide 66/montmorillonite nanocomposites. *Polymer*, **44**, 7533–7538.

Rutherford, D.W., Chiou, C.T., and Eberl, D.D. (1997) Effects of exchanged cation on the microporosity of montmorillonite. *Clays and Clay Minerals*, **45**, 534–543.

Sainz-Díaz, C.I., Timon, V., Botella, V., Artacho, E., and Hernández-Laguna, A. (2002) Quantum mechanical calculations of dioctahedral 2:1 phyllosilicates: Effect of octahedral cation distributions in pyrophyllite, illite, and smectite. *American Mineralogist*, **87**, 958–965.

Sato, T., Watanabe, T., and Otsuka, R. (1992) Effects of layer charge, charge location, and energy change on expansion properties of dioctahedral smectites. *Clays and Clay Minerals*, **40**, 103–113.

Skipper, N.T., Chang, F.-R.C., and Sposito, G. (1995a) Monte Carlo simulation of interlayer molecular structure in swelling clay minerals. 1. Methodology. *Clays and Clay Minerals*, **43**, 285–293.

Skipper, N.T., Chang, F.-R.C., and Sposito, G., (1995b) Monte Carlo simulation of interlayer molecular structure in swelling clay minerals; 2, Monolayer hydrates. *Clays and Clay Minerals*, **43**, 294–303.

Skipper, N.T., Refson, K., and McConnell, J.D.C. (1991) Computer simulation of interlayer water in 2:1 clays. *The Journal of Chemical Physics*, **94**, 7434–7445.

Skipper, N.T., Lock, P.A., Titiloye, J.O., Swenson, J., Mirza, Z.A., Howells, W.S., and Fernandez-Alonso, F. (2006) The structure and dynamics of 2-dimensional fluids in swelling clays. *Chemical Geology*, **230**, 182–196.

Slade, P.G., Quirk, J.P., and Norrish, K. (1991) Crystalline swelling of smectite samples in concentrated NaCl solutions in relation to layer change. *Clays and Clay Minerals*, **39**, 234–238.

Stucki, J.W. (1988) Structural iron in smectites. Pp. 625–675 in: *Iron in Soils and Clay Minerals* (J.W. Stucki, B.A. Goodman, and U. Schwertmann, editors). D. Reidel Publishing Co., Dordrecht, The Netherlands.

Suquet, H., de la Calle, C., and Pezerat, H. (1975) Swelling and structural organization of saponite. *Clays and Clay Minerals*, **23**, 1–9.

Suter, J.L., Boek, E.S., and Sprik, M. (2008) Adsorption of a sodium ion on a smectite clay from constrained ab initio molecular dynamics simulations. *The Journal of Physical Chemistry C*, **112**, 18832–18839.

Tambach, T.J., Hensen, E.J.M., and Smit, B. (2004) Molecular simulations of swelling clay minerals. *The Journal of Physical Chemistry B*, **108**, 7586–7596.

Timon, V., Sainz-Díaz, C.I., Botella, V., and Hernández-Laguna, A. (2003) Isomorphous cation substitution in dioctahedral phyllosilicates by means of *ab initio* quantum mechanical calculations on clusters. *American Mineralogist*, **88**, 1788–1795.

Tsipursky, I. and Drits, V.A. (1984) The distribution of octahedral cations in the 2:1 layers of dioctahedral smectites studied by oblique-texture electron diffraction. *Clay Minerals*, **19**, 177–193.

Tunega, D., Goodman, B.A., Haberhauer, G., Reichenauer, T.G., Gerzabek, M.H., and Lischka, H. (2007) Ab initio calculations of relative stabilities of different structural arrangements in dioctahedral phyllosilicates. *Clays and Clay Minerals*, **55**, 220–232.

Velde, B. (1995) *Origin and Mineralogy of Clays*. Springer-Verlag, New York.

Wan, C., Qiao, X., Zhang, Y., and Zhang, Y. (2003) Effect of different clay treatment on morphology and mechanical properties of PVC-clay nanocomposites. *Polymer Testing*, **22**, 453–461.

Whitley, H.D. and Smith, D.E. (2004) Free energy, energy, and entropy of swelling in Cs-, Na- and Sr-montmorillonite clays. *The Journal of Chemical Physics*, **120**, 5387–5395.

Zabat, M. and Van Damme, H. (2000) Evaluation of the energy barrier for dehydration of homoionic (Li, Na, Cs, Mg, Ca,

Ba, $Al_x(OH)_y^{z+}$ and La)-montmorillonite by a differentiation method. *Clay Minerals*, **35**, 357–363.

Zhang, Y.-H., Dang, Z.-M., Fu, S.-Y., Xin, J.H., Deng, J.-G., Wu, J., Yang, S., Li, L.-F., and Yan, Q. (2005) Dielectric and dynamic mechanical properties of polyimide-clay nanocomposite films. *Chemical Physics Letter*, **401**, 553–557.

(*Received 4 June 2009; revised 5 November 2009; Ms. 323; A.E. S. Petit*)